Accurate identification and quantification of commensal microbiota bound by host immunoglobulins

Matthew A. Jackson[1*], Claire Pearson[1], Nicholas E. Ilott[1], Kelsey E. Huus[2,3], Ahmed N. Hegazy[1,4], Jonathan Webber[1], B. Brett Finlay[2,3,5], Andrew J. Macpherson[6,7], Fiona Powrie[1], Lilian H. Lam[1]

1. Kennedy Institute of Rheumatology, University of Oxford, Oxford, UK
2. Michael Smith Laboratories, University of British Columbia, Vancouver, BC V6T 1Z4, Canada
3. Department of Microbiology and Immunology, University of British Columbia, Vancouver, BC V6T 1Z4, Canada
4. Department of Gastroenterology, Infectiology, and Rheumatology, Charité-Universitätsmedizin Berlin, Campus Benjamin Franklin, Berlin, Germany, Deutsches Rheumaforschungszentrum Berlin (DRFZ), an Institute of the Leibniz Association and Berlin Institute of Health (BIH), Berlin, Germany
5. Department of Biochemistry and Molecular Biology, University of British Columbia, Vancouver, BC V6T 1Z4, Canada
6. Maurice Müller Laboratories, Department of Biomedical Research, University of Bern, 3008 Bern, Switzerland.
7. University Clinic of Visceral Surgery and Medicine, Inselspital, 3010 Bern, Switzerland

* Corresponding author

1

Abstract

Background

Identifying which taxa are targeted by immunoglobulins can uncover important host-microbe interactions. Immunoglobulin binding of commensal taxa can be assayed by sorting bound bacteria from samples and using amplicon sequencing to determine their taxonomy, a technique most widely applied to study Immunoglobulin A (IgA-Seq). Previous experiments have scored taxon binding in IgA-Seq datasets by comparing abundances in the IgA bound and unbound sorted fractions. However, as these are relative abundances, such scores are influenced by the levels of the other taxa present and represent an abstract combination of these effects. Diversity in the practical approaches of prior studies also warrants benchmarking of the individual stages involved. Here, we provide a detailed description of the design strategy for an optimised IgA-Seq protocol. Combined with a novel scoring method for IgA-Seq datasets that accounts for the aforementioned effects, this platform enables accurate identification and quantification of commensal gut microbiota targeted by host immunoglobulins.

Results

Using germ-free and *Rag1*$^{-/-}$ mice as negative controls, and a strain-specific IgA antibody as a positive control, we determine optimal reagents and fluorescence activated cell sorting (FACS) parameters for IgA-Seq. Using simulated IgA-Seq data, we show that existing IgA-Seq scoring methods are influenced by pre-sort relative abundances. This has consequences for the interpretation of case-control studies where there are inherent differences in microbiota composition between groups. We show that these effects can be addressed using a novel scoring approach based on posterior probabilities. Finally, we demonstrate the utility of both the IgA-Seq protocol and probability-based scores by examining both novel and published data from *in vivo* disease models.

Conclusions

We provide a detailed IgA-Seq protocol to accurately isolate IgA-bound taxa from intestinal samples. Using simulated and experimental data, we demonstrate novel probability-based scores that adjust for the compositional nature of relative abundance data to accurately quantify taxon-level IgA binding. All scoring approaches are made available in the IgAScores R package. These methods should improve the generation and interpretation of IgA-Seq datasets and could be applied to study other immunoglobulins and sample types.

Background

The immunoglobulin isotype A (IgA) is secreted by plasma cells at mucosal barrier sites such as the gastrointestinal (GI) tract, which is also host to the densest community of commensal bacteria in the human body[1, 2]. Intestinal homeostasis requires tolerance to the microbiota but a robust defence against pathogens, and growing evidence suggests that IgA binding is both taxon-dependent and context-specific. IgA in the mucus layer forms a protective barrier between the epithelium and the luminal microbiota [3–5]. Some commensal bacteria have adapted to this specialized niche to promote homeostasis. *Bacteroides fragilis* produces a surface polysaccharide that promotes IgA binding and facilitates mucus layer colonization [6] and the mucin-degrader *Akkermansia muciniphila* induces host IgA and IgG responses[7]. Other studies have suggested that low-affinity IgA contributes to microbiota maintenance, while high-affinity IgA acts on pathogens to promote clearance and inhibit virulence [8–15]. Pathobionts are members of the microbiota that are typically harmless under homeostatic conditions but can drive disease given certain environmental stimuli[16]. IgA binding of taxa might also reflect such pathogenic potential and IgA bound gut bacteria have been implicated in inflammatory disease [17–20]. Accurate identification of commensal microbiota bound by IgA can therefore offer important insights into the mechanisms underlying host microbial mutualism and its dysregulation in disease.

Microbiota-wide profiling of IgA bound taxa can be achieved using IgA-Seq. Anti-IgA antibodies are used to stain a complex gut microbiota, then bound and unbound bacteria are separated by Fluorescence Activated Cell Sorting (FACS) or Magnetic Activated Cell Sorting (MACS) and identified by 16S rRNA gene sequencing [17, 18]. We refer to the sorted IgA bound bacteria as the IgA+ fraction, the sorted unbound bacteria as the IgA- fraction, and the sample before sorting as the pre-sort sample. IgA-Seq has been used to uncover antibody targeting of taxa by both T-cell dependent and T-cell independent pathways [7, 10, 12, 21, 22], as well as differential binding of taxa during disease. IgA-Seq was first described by Palm et al. to identify taxa differentially bound by IgA in inflammatory bowel disease (IBD) patients [17] and was adapted by Kau et al. to identify increased

3

97   binding of *Enterobacteriaceae* by IgA in malnourished infants [18]. Variations of these protocols

98   have since been applied to study IgA binding in other disease states, employing a range of IgA-Seq

99   protocols utilising different reagents, sort modalities and configurations [19, 20]. Some of these

100   parameters have been validated individually in prior studies but there has yet to be a comprehensive

101   description of how to design and benchmark an optimal IgA-Seq protocol.

102

103   More importantly, there has yet to be a formal consideration of the analytical approaches used to

104   score taxon binding in IgA-Seq datasets. IgA-Seq does not quantify the affinity of IgA antibodies

105   directly, but rather provides a measure of overall IgA binding. The likelihood of bacteria within a

106   given taxon being bound by IgA will be influenced by a combination of the affinities of the IgA pool

107   for the taxon, the spatial distribution of those bacteria, and the expression of relevant epitopes by the

108   taxon. Additionally, the IgA+ abundance does not solely represent this likelihood of taxon binding. It

109   is also a function of the number of bacteria present: a taxon highly targeted by host IgA could make

110   up a low proportion of the IgA+ fraction if only a few bacteria are present and vice versa. The

111   principal aim of IgA-Seq is not to solely identify which taxa are most bound by IgA but rather to

112   identify those taxa with a higher likelihood of binding relative to other bacteria. As a result, indices

113   that account for the initial quantities of bacterial taxa must be applied to quantify IgA-Seq data.

114

115   In IgA-Seq studies to date, IgA binding has largely been scored using indices as described by either

116   Palm et al. or Kau et al. (referred to here as the Palm and Kau indices for clarity)[17, 18]. These

117   scores compare the abundance of a taxon in the IgA+ fraction to its abundance in the IgA- fraction.

118   This accounts for the overall pre-sort quantities of taxa on the assumption that, as both fractions are

119   drawn from the same starting pool of bacteria, the IgA+ and IgA- abundances are representative of the

120   proportion of a taxon's bacteria bound by IgA. However, these scores are influenced by an additional

121   confounder – that these are relative abundances. As a result, an increase in one taxon will inherently

122   reduce the percentage contribution of others. Thus, the IgA+ and IgA- abundances of a given taxon

123   are also influenced by the starting abundances and IgA binding of all other taxa. Scores like the Kau

124   and Palm indices correlate with taxon-level IgA binding but the necessity to use relative abundances

125   in IgA-Seq experiments abstracts their interpretation. We will show that, without careful

126   consideration of these effects, it is possible to misinterpret results observed using these metrics.

127

128   Here, we aim to address these methodological and analytical limitations to improve the accessibility,

129   quality and quantitative interpretation of IgA-Seq experiments. Using germ-free and immune-

130   deficient mice as negative controls and a strain-specific IgA antibody for positive controls, we

131   describe the methods that can be used to validate the quality of each stage of an IgA-Seq experiment

132   and derive an optimised IgA-Seq protocol. In lieu of a gold standard for benchmarking IgA binding

133   scores, we develop a platform for simulating an IgA-Seq experiment where the underlying relative

134   IgA binding levels between taxa are known. Using this, we show that existing indices used to score

135   taxon-level IgA binding are influenced by relative abundances, which needs to be taken into account

136   when drawing conclusions. We present novel probability-based scores that circumvent this by

137   providing direct quantification of the proportion of bacteria belonging to a given taxon that are bound

138   by IgA. Finally, we demonstrate the utility of the protocol and novel probability scores by applying

139   them to study IgA binding in mouse models of colitis and malnourishment. These methods facilitate

140   generation of high-quality IgA-Seq data and direct quantification of relative immunoglobulin binding

141   between taxa.

142

143   **Results**

144

145   **Quality control standards for bacterial flow cytometry and IgA staining**

146

147   We first determined the optimal gating strategy for isolating bacteria from faecal and colonic samples

148   by FACS. The BD LSRFortessa X20 and FACSAria III flow cytometers were selected based on an

149   identical configuration with 405, 488, 633 and an additional 561nm laser, which eliminated PE-FITC

150   spill over and increased PE sensitivity. Whereas eukaryotic cells have diameters ranging from 10–100

151   microns, bacteria generally range from 0.3–5 microns, though some can vary by two orders of

152   magnitude and have variable width to height ratios. In stock configurations, both these cytometers use

5

153   a sensitive PMT to detect SSC, and therefore a minimum SSC threshold was used to fully capture a

154   wide range of particle sizes.

155

156   Bacteria must then be distinguished from small debris particles in the buffers and the sample itself,

157   particularly in faecal samples which contain substantial autofluorescent debris. Cell-permeable SYBR

158   Green I nucleic acid stain identified bacteria in samples from specific pathogen-free (SPF) mice but

159   did not stain filter-sterilized FACS buffer (Fig. S1A). Nucleic acid staining may be variable amongst

160   diverse bacteria. This is because there may be differences in cell permeability and transport

161   mechanisms, the size and/or number of copies of genomic DNA, and any individual cell may be

162   undergoing asymmetric division. These could produce a wide distribution of SYBR staining

163   intensities. To ensure these are captured whilst minimising contaminating debris, stool from germ-free

164   (GF) mice and unstained SPF stool was used to define SYBR+ gating parameters specific for bacteria

165   (Fig. S1A).

166

167   Next, we sought to validate the specificity of the PE-conjugated rat anti-mouse IgA (mA-6E1)

168   antibody that would be used in downstream IgA-Seq experiments. To do this we used IgA deficient

169   mice as negative controls and a strain specific IgA antibody as a positive control. SPF $Rag1^{-/-}$ mice

170   have a complex microbiota but lack T cells and mature B cells responsible for the production of IgA.

171   Essentially no bacteria were stained by the PE anti-mouse IgA antibody in samples from $Rag1^{-/-}$ mice

172   compared to roughly 4% of the microbiota in wild-type SPF mice (Fig. S1B). To further confirm the

173   specificity of the IgA antibody, we replicated the approach of Kau et al. [18], using an *in vitro* system

174   with an artificial 2-member bacterial community in which only one strain should be stained by PE

175   anti-mouse IgA. *Bacteroides thetaiotaomicron* (*B. theta*), a common commensal of the murine gut,

176   was coated with a mouse IgA antibody specific to the *B. theta* strain VPI-5482 [23]. *Escherichia coli*

177   was coated with a mouse IgG antibody as a control and mixed with the labelled *B. theta* prior to

178   staining with the PE anti-mouse IgA antibody. Flow cytometry revealed that a proportion equivalent

179   to the expected *B. theta* population was stained by the PE anti-mouse IgA antibody (Fig. S1C),

180   confirming the specificity of the antibody to be used in downstream IgA-Seq experiments. The gating

6

181   strategy used for the IgA-Seq protocol (Fig. 1A) was validated using these SYBR and IgA staining

182   controls.

183

184   **A benchmarked protocol for IgA-Seq**

185

186   The goal of IgA-Seq is to isolate bacterial populations coated by endogenous host IgA and to identify

187   them by 16S rRNA gene sequencing. To this end, it is critical to identify FACS parameters that

188   maximise the integrity and purity of sorted samples. Using *B. theta* as a model commensal anaerobe, a

189   culture-grown suspension of *B. theta* was once again labelled with strain-specific IgA and PE anti-

190   mouse IgA, and 100 cells were sorted as an array onto an agar plate to determine viable colony

191   forming units (CFU). The default cytometer settings for 100 and 85 micron nozzles were tested, in

192   addition to a custom 30 psi configuration for the 85 micron. Intact bacterial recovery decreased with

193   smaller nozzles sizes and higher pressures, and viability was enhanced by sorting at the lower 30 psi

194   pressure on the 85 micron nozzle (Fig. 1B). Only 20% of bacteria could be recovered with the 70

195   micron nozzle (Fig. 1B), which was discontinued from further testing.

196

197   To test the sort fidelity of the fractions produced by each of the configurations, we sorted IgA+ and

198   IgA- bacterial populations from SPF mouse stool (Fig. 1A). These fractions were then analysed using

199   the same parameters to determine the percentage of bacteria that were retained within defined sort

200   gates. All three FACS configurations enabled >90% sort purity for both IgA+ and IgA- fractions (Fig.

201   1C). This is in contrast to magnetic activated cell separation (MACS), an alternative sorting modality

202   which performed poorly with purities of 37.1– 42.9% for the IgA+ fraction (Fig. 1D-E). The FACS

203   configuration utilising the 100 micron nozzle produced the highest sort purities in both IgA+ and IgA-

204   fractions, followed by the 85 micron nozzle at 30 psi (Fig. 1C). Practically, the low pressure required

205   for the 100 micron nozzle reduces the flow rate and throughput by ~70%. Given that a minimum of

206   400,000 cells are required per fraction for downstream sequencing applications, the 85 micron with 30

207   psi configuration is vastly more time effective while maintaining high viability and sort purities. We

208   also found this configuration allowed for sensitive sort control that, if desired, allows for finer grain

209   collection of IgA+ subpopulations for instance IgA$^{\text{bright}}$ and IgA$^{\text{dim}}$ fractions (Fig. S2). This

210   configuration was selected for downstream IgA-Seq.

211

212   As a final test of the precision of our sorting approach, we devised an experiment to specifically

213   isolate an IgA+ strain from a complex stool microbiota. We once again took advantage of our ability

214   to coat *B. theta* with mouse IgA in a strain-specific manner, which we stained separately before

215   spiking into an unstained faecal suspension prepared from SPF wild-type mice (Fig. 2A). Endogenous

216   IgA-coating of faecal microbiota remained but as the faecal suspension was not stained only the PE

217   anti-mouse IgA stained *B. theta* culture should be isolated with this approach. *B. theta* comprised

218   roughly 12.5% of the whole community in the spiked stool mixture, and high sort purities were

219   achieved for both the IgA+ (97.4% – 99.4%) and IgA- fractions (97.3% – 100%) across three

220   replicate sorts Figure 2B). 16S rRNA gene sequencing was performed on the complex stool

221   community prior to the addition of *B. theta*, and in addition to the IgA+ fractions after three sorts from

222   the same spiked sample. Genomic DNA from *B. theta* was included as a positive control. As a

223   contamination check, sheath fluid was also included but it contained little DNA and did not produce a

224   viable library. The IgA+ fractions were comprised almost entirely of *B. theta* (98.4 – 99.6%; Figure

225   2C-D) and lacked any additional unstained taxa observed in the complex community. This

226   demonstrates that our optimised protocol can sort IgA bound bacteria from a complex gut microbiome

227   with high accuracy.

228

229   **Pre-sort taxonomic abundances influence existing IgA binding scores**

230

231   Once a sample has been sorted, amplicon-based sequencing of extracted DNA from the sort fractions

232   is used to determine the relative abundances of the taxa within them. As discussed previously (see

233   Background), the abundance of a taxon in the IgA+ fraction is a function of both its likelihood of IgA

234   binding and its overall abundance in the pre-sort community. As we are principally interested in the

235   former, we must use scoring metrics to quantify the relative IgA binding of taxa whilst taking their

236   pre-sort abundances into account. To date, this has principally been achieved using indices that

8

237   compare taxon abundances in the IgA+ and IgA- fractions and two such indices have been described -

238   the Palm and Kau indices (see Methods). Using a toy example where two samples have identical IgA

239   binding affinities for two species but differ in their starting abundances, we can see that these scores

240   are still influenced by pre-sort abundances and produce different affinity scores for each sample (Fig.

241   3A). This is because these scores do not account for the fact that abundances are relative measures

242   and thus the starting abundance and IgA binding of all other taxa will also influence the observed

243   abundance of a given taxon in the sorted fractions.

244

245   If we instead consider the IgA+ relative abundance as the probability of a taxon being within the IgA+

246   fraction, it is possible to apply Bayes' theorem to derive a posterior probability of IgA binding for

247   each taxon, i.e. the probability that a given bacterium will be bound to IgA given that it belongs to a

248   given taxon (see Methods for a more detailed discussion). In our example, this posterior probability is

249   not influenced by the starting abundances and provides a direct quantification of the likelihood of IgA

250   binding for each taxon (Fig. 3A). Here, we describe two scoring methods based on these posterior

251   probabilities: 1) The IgA+ probability - using the positive fraction probability directly and 2) The

252   Probability Ratio – the ratio of the IgA+ and IgA- probabilities (see Methods).

253

254   **Probability-based scores accurately recapitulate relative IgA binding in simulated data**

255

256   As the true level of IgA binding to each bacterial taxon cannot be measured directly *in vivo*, we

257   created a platform to simulate an IgA-Seq experiment *in silico* to benchmark scoring methods. This

258   allowed IgA-Seq data to be generated with pre-defined relative levels of IgA binding between species.

259   In each simulation we maintain the relative level of IgA binding for each species across all samples

260   and only change the pre-sort abundances of species. This allows us to determine how robust scoring

261   methods are to these effects. A perfect scoring method should produce identical IgA binding scores

262   for each species across all samples, with a relative ranking of IgA binding between species that

263   matches the pre-defined levels.

264

9

265   Ten species were simulated, each having a unique normal distribution of IgA binding. IgA binding

266   was represented by an arbitrary value that just represents the relative levels of binding between taxa

267   (Fig. 3B). 30 samples were generated each containing 100,000 bacteria. The bacteria were assigned to

268   each of the ten species randomly to produce different log distributed starting abundances for each

269   sample (Fig. 3C). Each bacterium in each sample was then assigned an IgA binding value by

270   sampling from the distribution of its species. Bacteria whose binding values were above four were

271   considered IgA+ and those below two in the IgA- fraction. These thresholds were chosen based on the

272   overall distribution of IgA values to mimic the extremes selected in a typical IgA-Seq experiment

273   (Fig. 3B). The number of bacteria in each sample's IgA+ and IgA- fraction was used to determine the

274   size of the fractions and the species counts were converted to taxonomic relative abundances (Fig.

275   3C). These values were in turn used to derive the various IgA binding scores.

276

277   Samples had different IgA+ and IgA- fraction sizes, defined as the percentage of total bacteria within

278   the fraction, due to their different initial taxonomic compositions and the differing IgA binding of the

279   ten species (Fig. 3D). Given that each taxon's IgA binding was constant across samples, we would

280   expect there to be no variation across samples if an IgA binding score properly adjusts for the

281   differences in sample composition. Comparing the consistency of scoring methods across samples, the

282   IgA+ Probability had a significantly lower coefficient of variation than the Palm index and the

283   Probability Ratio had significantly lower variation than all other scores. The probability-based

284   methods were more consistent than the Palm and Kau indices, and thus less influenced by the

285   differences in pre-sort abundances between samples (Fig. 3E).

286

287   When considering the relative rankings of the species, all four scoring methods were significantly

288   correlated with the true IgA binding affinities and ranked species in the correct order of IgA binding

289   (Fig. 3F). However, the Palm and Kau indices had a lower correlation than either of the probability-

290   based methods due to the larger variation between samples. Comparing the results of Pearson and

291   Spearman correlations, it is apparent that the Kau and Probability Ratio scores produce a more linear

292   distribution than the other two methods. This is due to their consideration of both the IgA+ and IgA-

293   fractions, which is not in the case in the IgA+ Probability, and taking the log to centre the score,

294   which is not the case in the Palm index or IgA+ Probability. Overall in this initial simulation,

295   probability-based methods proved robust to the influences of pre-sort abundances, which introduced

296   variability to the Palm and Kau indices. The Probability-Ratio almost perfectly recapitulated the

297   relative relationships of the true IgA binding values.

298

299   **Probability-based methods overcome biases effecting the interpretation of between group**

300   **comparisons**

301

302   The Kau and Palm indices showed variation in scores due to differences in pre-sort abundances. This

303   could be particularly problematic when comparing IgA binding between groups that have inherent

304   and consistent differences in microbiome composition. This is likely, as a key use-case for IgA-Seq is

305   to determine if previously established microbiome differences between groups, such as healthy

306   controls and disease patients, are being driven by differential targeting of the IgA pool.

307

308   To determine the effects of pre-sort abundance biases on inter-group comparisons, we repeated the

309   simulation but divided samples into a case and control group. The simulation was run with 30 samples

310   per group each containing ten species with the same underlying IgA affinities as before (Fig. 3B).

311   Random initial abundances were then generated as previously but additional Species 10 (with a

312   moderate IgA affinity value) was introduced to the 30 case samples – simulating outgrowth of one

313   specific taxon in a disease. In this simulation, as before, an optimal scoring approach will not detect

314   any differences between the cases and controls whose species share the same IgA binding and only

315   differ in their pre-sort abundances.

316

317   As expected, Species 10 constituted a larger percentage of the relative abundances in both the IgA+

318   and IgA- fractions of the cases compared to the controls (Fig. 4A). This led to a significantly higher

319   IgA- fraction size in the control group when compared to cases but no difference in the IgA+ fraction

320   sizes (Fig. 4B). Comparing the overall distribution of scores, there was greater variability across

11

321   samples in the Kau index than the Probability Ratio, and Species 10 IgA binding estimates were

322   higher in cases using the Kau index (Fig. 4C). When testing differences between the simulated case

323   and control groups, the Kau index inferred significant differences in the IgA binding of both Species

324   10 and Species 6 where there should be none (Fig. 4D). This is an artefact of measuring relative

325   abundances. In the simulated disease cases there was an increased abundance of Species 10 in the

326   IgA+ fraction. This reduces the relative contribution of Species 6 (the highest affinity taxa that would

327   otherwise constitute the majority of the IgA+ fraction) and alters the ratio when calculating the Kau

328   score. No significant differences were observed using the Palm index but this only resolved the highly

329   bound Species 6, which displayed increased variance in the controls (Fig. S3). The Probability Ratio

330   resolved both high and low IgA binding of taxa and was more resistant to the influence of the pre-sort

331   abundances, maintaining similar estimates between cases and controls (Fig. 4D).

332

333   **IgA-Seq in a mouse model of colitis produces different outcomes across scoring methods**

334

335   To demonstrate the utility of our benchmarked IgA-Seq protocol we applied it to study commensal

336   IgA binding in a mouse model of colitis. *Helicobacter hepaticus* (*Hh*) can inhabit the murine

337   intestinal tract without harm but can emerge as a pathogen when host immune responses are

338   dysregulated as a result of either genetic susceptibility or targeted immunomodulation [24].

339   Abrogation of anti-inflammatory IL-10 signalling by administration of an anti-IL10 receptor antibody

340   (aIL10R) results in *Hh*-driven colitis[25]. We recapitulated this model in a gnotobiotic C57BL/6

341   mouse colony stably colonized with a 12-member microbiota (MM12) that recapitulates the

342   taxonomic diversity of a more complex community[26]. This provides a defined minimal microbiota

343   to specifically interrogate IgA binding.

344

345   Control MM12 mice treated solely with weekly aIL10R injections did not develop any pathology

346   (Fig. 5A). In contrast, MM12 mice that received aIL10R in conjunction with *H. hepaticus* infection

347   (*Hh*+aIL10R) developed marked inflammation and colitis after 14 days (Fig. 5A). Lipocalin-2,

348   released by activated neutrophils and a biomarker for inflammation[27], was also elevated in the

349   colon contents of *Hh*+aIL10Rmice but not control aIL10R only mice, whose lipocalin-2 levels were

350   similar to steady-state mice lacking aIL10R injection (Fig. 5B). There was a significant increase in

351   IgA-coating of colonic bacteria from colitic mice (Fig. 5C-D). Colonic contents from both control and

352   colitis groups were subjected to IgA-Seq to identify taxa targeted during inflammation.

353

354   Taxa were profiled in the pre-sort samples and the IgA+ and IgA- fractions using 16S rRNA gene

355   sequencing. Analyses were carried out at the level of species summarised amplicon sequence variants

356   (ASVs). Using the V4 16S rRNA gene region we were able to distinguish almost all members of the

357   MM12 and *Hh* either by species level assignment or sole membership of a genus (Table S1). The

358   exception were two closely related *Clostridium* species that were both assigned to *Clostridium XlVa.*

359   A blank sequencing control was used to identify potential contaminants introduced at the DNA

360   extraction and library preparation stage. Given that we used mice with a defined microbiota, we were

361   also able to determine the presence of contaminants introduced elsewhere. After removing taxa

362   observed in the blank control, several unexpected (non-MM12 or *Hh*) species remained (Fig. S4A).

363   The majority of these were at a lower abundance than the expected species across all samples. These

364   were removed from later analyses using an abundance threshold chosen to remove rare taxa whilst

365   retaining the majority of total observations (Fig. S4B). It is of note that contaminant taxa were far

366   more predominant in the sorted IgA+ and IgA- fractions. This may be due to the lower biomass in

367   these samples but could also be due to species being introduced during sorting or library preparation.

368   These were accounted for by additional screening to only retain species observed in the pre-sort

369   sample for each mouse, which led to no unexpected taxa being observed in any sample (Fig. S4C).

370   Thus, we recommend using abundance thresholding followed by validation against pre-sort samples

371   to filter taxa prior to scoring in IgA-Seq analyses.

372

373   After quality control, *Hh* was detected in the whole and IgA+ fractions of all four *Hh*+aIL10R mice

374   and samples clustered clearly by both experimental condition and sort fraction (Fig. 5E-F). *Hh* was

375   also detected in the pre-sort sample in one of the aIL10R only mice, but as this was not detected in

376   either the IgA+ or IgA- fractions it ultimately did not influence the IgA binding scores for this mouse.

377 We compared the different IgA binding scores across all mice, focusing on the methods that included

378 both the IgA- and IgA+ fractions. All methods broadly ranked species IgA binding in the same order

379 and there was a significant positive correlation between all scores (Fig. S5A). The Kau index and

380 Probability Ratio shared the strongest correlation, with the main difference between the two being a

381 more even distribution of values within the Probability Ratio than in the Kau index, which contained

382 isolated peaks of scores where taxa were predominantly observed in the IgA+ or IgA- fraction (Fig.

383 S5A).

384

385 When comparing species IgA binding scores between groups, the method used had important and

386 distinct effects on the interpretation of the results. All methods identified significant differences in

387 IgA binding of *Clostridium* between the *Hh*+aIL10R and aIL10R only treatments (Fig. 5G, Fig. S5B).

388 This was the largest effect observed and was clearly detected by all three methods in the same

389 direction with an increased IgA binding of *Clostridium* in colitic mice. Some taxa, such as

390 *Enterococcus,* were only observed in the IgA+ and/or IgA- fractions in the colitic mice. It was

391 therefore not possible to compare their binding relative to the control mice. This highlights the need to

392 additionally observe presence/absence patterns of taxa in the fractions alongside using quantitative

393 scoring methods.

394

395 The Kau index and Probability Ratio additionally detected a significant difference in IgA binding to

396 *A.muciniphila* between the groups. However, the Kau and Palm scores were lower for *A.muciniphila*

397 in colitic mice, whereas the Probability Ratio was higher (Fig. 5G). This discrepancy results from the

398 large contribution of *Hh* to the relative abundances in the IgA+ fraction of the colitis group. This

399 inherently reduced the observed relative abundance of *A. muciniphila* in this fraction even in the

400 absence of a change in the absolute levels bound to IgA. This is less pronounced in the IgA- fraction

401 (where less *Hh* is observed) and thus the overall IgA+/IgA- ratio of *A. muciniphila* was reduced (Fig.

402 5G). However, even though *A. muciniphila* accounts for a reduced percentage of the IgA+ fraction,

403 the total IgA+ fraction is much larger in the colitic mice (Fig. 5H). A smaller percentage of this much

404 larger total IgA+ fraction actually represents a larger total amount of *A. muciniphila* bound to IgA in

405   the colitic group (Fig. 5H). Thus the Probability Ratio, which accounts for the fraction sizes, infers a

406   positive rather than negative shift in IgA binding of *A.muciniphila*. This highlights the benefit of

407   using probability-based metrics that provide a direct estimate of the likelihood of IgA binding for

408   each taxon in comparison to solely abundance-based indices, which might lead to a conflicting

409   interpretation without careful consideration of what the scores represent.

410

411   **The Probability Ratio increases power to detect differences in IgA binding between conditions**

412

413   As an additional test of the Probability Ratio we applied it to a published IgA-Seq dataset with

414   extensive experimental evidence to support differences in IgA binding between conditions. Huus et al.

415   used FACS-based IgA-Seq to study bacterial binding of GI IgA in a mouse model of nutrient

416   restriction [20]. Mice on a conventional (CON) or moderately malnourished diet (MAL) were tracked

417   from weaning to adulthood. Applying the Kau index, they found that mice on a conventional diet

418   develop increased binding of *Lactobacillus* as they age from three to seven weeks old, whereas

419   malnourished mice do not. They observed this effect to be consistent across different sites in the GI

420   tract and confirmed it was driven by differential binding of IgA to *Lactobacillus* using ELISA. This

421   provided an ideal dataset to test the robustness of the Probability Ratio.

422

423   Huus et al. provided processed 16S rRNA gene sequencing data generated from faecal samples used

424   in their study and the associated IgA+ and IgA- fraction sizes, which had been recorded for a subset

425   of the original data [20]. This enabled the Probability Ratio to be calculated for samples from four

426   CON and MAL mice at each of the three ages. The Kau score (used in the original study) was also

427   calculated as a comparator.

428

429   Comparing between diet and ages using the Kau index, we identified five taxa with differential IgA

430   binding (Fig. 6A). *Lactobacillus* was the only taxon significantly different by the interaction of age

431   and diet and reflected the patterns observed previously. Three taxa, *Lactococcus* and unclassified

432   *Lachnospiraceae and Erysipelotrichaceae*, displayed increased IgA binding in MAL mice. All three

15

433   of these taxa were observed with the same association in the original analysis of the dataset. We

434   additionally observed a reduced IgA binding of *Roseburia* at three week old MAL mice. This was not

435   reported in the Huus et al. analysis using the Kau index. However, due to the smaller sample size

436   available we explicitly targeted our testing to between group effects and the prior analysis did not.

437

438   Carrying out similar modelling using the Probability Ratio to score IgA binding, we reproduced all of

439   the associations identified using the Kau index with the exception of the unclassified

440   *Erysipelotrichaceae* taxon, which was no longer significantly different between groups (Fig. 6B).

441   Across all of the other associations detected as significant by either the Kau Index or Probability

442   Ratio, the Probability Ratio consistently produced lower p-values (Fig. 6C, left). This reflects an

443   increased magnitude in the differences between the mean scores of the MAL and CON groups in most

444   comparisons when using the Probability Ratio compared to the Kau index (Fig. 6C, right). This can in

445   part be attributed to a reduced variation in taxon scores within groups when using the Probability

446   Ratio (Fig. 6D), as was also observed in the simulated data (Fig. 3E). This increased power is an

447   additional benefit of accounting for the size of the IgA+ and IgA- fractions when scoring IgA-Seq

448   data.

449

450   **Discussion**

451

452   The development of IgA-Seq has enabled powerful, unbiased investigation of immune interactions

453   between host and commensal microbiota. As this technique gains wider adoption, it is critical to

454   benchmark experimental and analytical approaches to ensure accurate quantification and

455   interpretation of IgA targeting. To this end, we provide an optimised IgA-Seq protocol and novel

456   scoring approaches that facilitate accurate identification of IgA coated bacteria. We developed a

457   simulation platform that enabled the first formal testing of IgA-Seq scores. This revealed that existing

458   scoring approaches are influenced by relative abundances and, without careful consideration, can lead

459   to the inference of alternate IgA binding patterns solely as a result of pre-sort abundance shifts.

460   Instead, we have developed new probability-based scoring methods that overcome these limitations

461   by directly quantifying of the likelihood of a taxon being bound by IgA. Importantly, as we have

462   showed in both simulated and *in vivo* datasets, these probability-based scores provide increased power

463   to detect differences in IgA binding between groups and promote accurate interpretation of IgA

464   targeting of taxa in health and disease states.

465

466   Analysis of *in silico* and *in vivo* datasets revealed that it is critical to properly account for both the

467   pre-sort taxonomic composition of a sample and the relative nature of fraction abundances when

468   comparing IgA targeting between case and control groups. Scoring indices that neglect to do so can

469   infer artificial and/or conflicting shifts in IgA binding estimates between experimental groups.

470   Simulating consistent group-wise shifts in pre-sort abundances resulted in significant differences in

471   taxon level binding estimates when using the Kau index. It is not that the Kau scores are incorrect, but

472   rather that they represent an abstract combination of both the IgA binding and abundance of the taxon

473   scored, and the IgA binding and abundance of all other taxa in the sample. This inherently

474   complicates their interpretation. In contrast, the probability-based scores adjust the taxonomic

475   abundances by the number of bacteria in IgA+ and IgA- fractions. This overcomes the relative nature

476   of quantification, which removes the influence of other taxa, and allows for proper adjustment for pre-

477   sort composition. As a result, probability-based scores provide a direct measure of the likelihood that

478   a bacterium is bound to IgA given that it belongs to a specific taxon. As shown with the increased

479   binding of *A.muciniphila* in the colitis model, this simplifies the interpretation of between group

480   changes in IgA binding when using the Probability Ratio.

481

482   Aside from artefacts that arise in between-group comparisons, all scoring indices were correlated

483   when considering global patterns across samples. This suggests that taxa ranked as generally highly

484   bound in previous studies are unlikely to change if quantified using the novel probability-based

485   scores. However, we found that the influence of pre-sort taxonomic composition meant there was

486   higher variability between samples when using the Kau and Palm scores compared to the probability-

487   based methods. This increased variance reduces the power to detect effects in experimental data and

488   resulted in a moderate increase in power when applying the Probability Ratio to the Huus et al. data.

489   Maximising power by using probability-based metrics is particularly desirable given the high

490   investment of experimental time required to generate IgA-Seq data, which can introduce a practical

491   limit on sample sizes.

492

493   Our work highlights the importance of selecting scores based on the underlying biological question.

494   If the primary interest is to simply identify which taxa have the most bacteria bound by IgA, then the

495   IgA+ abundance of a taxon can be used directly. If the purpose is to identify which taxa are being

496   more/less preferentially bound over other taxa, which is arguably more relevant when studying IgA

497   targeting, then probability-based scores that account for the relative nature of taxonomic abundances

498   should be used (Fig. S6). To select between using the IgA+ Probability or Probability Ratio: if the

499   sole interest is to identify taxa most likely to bind IgA then the IgA+ Probability is sufficient and

500   benefits from its direct interpretability as a probability of IgA binding (ranging from 0-1); otherwise

501   the Probability Ratio provides a more generally applicable score that also provides better resolution of

502   relative binding between taxa with lower IgA binding. For example, detecting the loss of

503   *Lactobacillus* binding in undernourished mice detected in the Huus et al study[20]. The Probability

504   Ratio additionally benefits from being centred on zero, so a positive or negative score indicates if the

505   majority of a taxon's bacteria fall into the IgA+ or IgA- fraction respectively. Score choice might also

506   be based on available sequencing data. The IgA+ Probability requires sequencing of the IgA+ fraction

507   and the pre-sort sample and the Probability Ratio requires sequencing of the IgA+ and IgA- fraction.

508   However, sequencing of both the IgA+ and IgA- fractions and the pre-sort sample has often been

509   applied in previous studies [17, 18]. As we have shown here, this provides additional benefits in the

510   detection of contaminants introduced by sorting and overall compositional differences between

511   experimental groups.

512

513   We have also presented an optimised IgA-Seq protocol that enables precise separation of IgA+ and

514   IgA- gut microbiota, and their cultivation to support subsequent interrogation in gnotobiotic disease

515   models and/or strain phenotyping. Our FACS-based protocol outperformed MACS in sort purity and

516   benefits from innate quantification of the IgA+ and IgA- fraction sizes required to calculate the

517   Probability Ratio. We employed a protocol design strategy that combined individual approaches

518   applied in previous studies including the controls used for validation of the staining and gating

519   strategy [18, 28]. To minimize technical variation between experiments, regular instrument calibration

520   alongside staining controls and gating templates should be employed. We utilised the same antibody

521   lot for all experiments within this study, but staining controls and gating strategies need to be verified

522   in instances of lot-to-lot variation. In addition, we developed a novel positive control approach to

523   testing protocol accuracy by successfully isolating pure IgA-bound *B. theta* from a complex intestinal

524   microbiota. While access to specific flow cytometers may vary, the concepts in experimental design

525   presented herein can be applied to validate IgA-Seq protocols on different sort modalities.

526

527   Similar approaches to IgA-Seq have also been used to study other isotypes, such as IgM and IgG[22,

528   29–31], and immunoglobulins isolated from other sites, for example quantifying GI bacteria bound by

529   serum IgA[32]. Expanding beyond IgA targeting of the gut microbiota, in future work, our protocol

530   design strategy and scoring approaches could be applied to investigate other sample types and

531   immunoglobulins. Further work could also be done to explore other variables influencing IgA

532   binding scores. For example, amplicon-based taxonomic abundances are inherently influenced by

533   PCR biases, differences in 16S rRNA gene copy number, and the taxonomic resolution of the variable

534   region amplified[33–35]. However, these are more general limitations of 16S rRNA gene sequencing

535   and their impact should be minimised assuming they occur uniformly in the IgA+ and IgA- fraction.

536   Mock sorts have previously shown that the sorting process itself has little influence on community

537   structure[17].

538

539   Technical variation in the isolation of IgA+ bacteria will also influence IgA binding estimates. For

540   example, using a more sensitive anti-IgA antibody or setting wider IgA+ gating in FACS will increase

541   the size of the IgA+ fraction and inherently increase the likelihood a taxon will be IgA+. This will not

542   influence relative scoring between taxa within a sample but it is important to maintain these variables

543   across samples in an experiment and/or consider randomisation of samples across technical batches to

544   avoid confounding of experimental groups. For similar reasons, absolute score values from any

545   method are unlikely to be analogous between experiments, however the relative rankings of taxa

546   should remain comparable. IgA-Seq is additionally limited to scoring relative, overall, IgA binding

547   between taxa. Understanding what drives the observed differences, such as alterations in the spatial

548   distribution of bacteria or changes in the affinities of host IgA, requires additional targeted

549   experiments, such as fluorescence *in situ* hybridisation and enzyme-linked immunosorbent assays[10,

550   20].

551

552   We have developed an optimised experimental protocol and novel scoring methodologies for IgA-

553   Seq. These enable robust and accurate identification of commensal bacteria targeted by the host

554   immune response. The IgAScores R package facilitates the application of these scores and we have

555   presented a guiding framework for selecting appropriate metrics. Furthermore, its simulation platform

556   will aid the future development of IgA-Seq analytics. This work enhances the accessibility and quality

557   of IgA-Seq studies, which should consequently uncover novel mechanistic insights into host-

558   microbiota interactions and the microbial drivers of health and disease.

559

560   **Conclusion**

561

562   Existing methods used to score taxon-level IgA binding in IgA-Seq experiments are influenced by the

563   initial taxonomic composition of samples and the relative nature of their quantification. This inflates

564   the variability in these scores and can have important consequences in between-group comparisons,

565   where scores might infer false or contrasting associations as a result of systematic differences in

566   microbiome composition between groups. Probability-based IgA scores can be used that overcome

567   this by providing a direct estimate of the likelihood a bacterium will be bound by IgA given its

568   taxonomy. These scoring methods are available in the IgAScores R package. Combined with the

569   practical approaches described here, these analytical developments enhance our ability to study taxon-

570   level immunoglobin binding of commensal microbiota; by increasing the power to detect associations

571   through reduced variability across samples and by providing an accurate, direct, quantification of

572   taxon binding from IgA-Seq data.

573 **Methods**

574

575 **Indices for scoring relative IgA binding of taxa in IgA-Seq experiments**

576

577 *Palm index*

578

579 In Palm *et al.*'s initial description of IgA-Seq they simply used the ratio of a taxon's IgA+ to IgA-

580 abundance in a score termed the IgA coating index[17]. Here, for clarity, we refer to this as the Palm

581 index ($Palm$). If IgA^+ and IgA^- represent taxon abundances in the respective fractions, for taxon i in

582 sample j the Palm index is defined as in Equation 1, where if IgA_{ij}^- is equal to zero a pseudo count (c)

583 is added to negate division by zero. Throughout we use a pseudo count of a similar magnitude but

584 below the smallest abundance observed in any sample.

585

586

$$Palm_{ij} = \frac{IgA_{ij}^+}{IgA_{ij}^-} \tag{1}$$

588

589

590

591 *Kau index*

592

593 Kau *et al.* described the IgA index, which is also solely based on IgA+ and IgA- relative abundances

594 [18]. It uses log transformation to make scores more comparable between taxa and considers the

595 difference of the IgA+ and IgA- abundances relative to their total. This has the benefit of centering the

596 score such that positive and negative values reflect overall higher abundances in the IgA+ or IgA-

597 fractions respectively. Using notation as previously, the Kau index (Kau) is defined as in Equation 2.

598

599

600
$$Kau_{ij} = -\frac{\log(IgA_{ij}^+ + c) - \log(IgA_{ij}^- + c)}{\log(IgA_{ij}^+ + c) + \log(IgA_{ij}^- + c)} \qquad (2)$$

601

602

603 *IgA+ Probability*

604

605 The relative abundances of taxa in a fraction or pre-sort sample sum to one. These can be considered

606 as probabilities. For example, taxa abundances in the pre-sort sample represent the probability that

607 any given bacterium in the sample belongs to a given taxon. The abundances in the IgA+ and IgA-

608 fractions can be considered as conditional probabilities (i.e. the probability of event A given that B

609 has occurred). For instance, IgA+ abundances represent the probability a bacterium belongs to a taxon

610 given that it is sufficiently bound to IgA to be in the IgA+ gate. In the case of IgA-Seq we are

611 interested in the inverse: the probability that a bacterium will be IgA+ if it belongs to a given taxon.

612 This is a posterior probability and can be calculated following Bayes' theorem (Equation 3).

613

614
$$P(A|B) = \frac{P(B|A)P(A)}{P(B)} \qquad (3)$$

615

616

617 Where $P(A|B)$ is the posterior probability that a bacteria is IgA+ given that it is from a chosen taxon.

618 $P(A)$ is the probability that any bacterium is bound to IgA sufficiently to be in the IgA+ fraction –

619 measured as the percentage of bacteria that fall within IgA+ FACs gate. $P(B)$ is the probability that a

620 bacterium will belong to a given taxon – measured as the taxon's relative abundance in the pre-sorted

621 sample. $P(B|A)$ is the probability a bacteria belongs to the taxon given that it is in the IgA+ fraction –

622 measured by the taxon's IgA+ abundance. In which case, the posterior probability ($Prob^{IgA^+}$) for

623 taxon i in sample j is defined as in Equation 4.1. Where $FracSize$ equals the fraction of sorted

624 bacteria in the IgA+ gate and $PreSort$ equals taxon abundances in the pre-sorted sample.

625

626
$$Prob_{ij}^{IgA^+} = \frac{IgA_{ij}^+ FracSize_j^{IgA+}}{PreSort_{ij}}$$
(4.1)

627

628

629 This measure will be referred to as the IgA+ Probability. The numerator provides a direct estimate of

630 the proportion of initial bacteria bound to IgA and should theoretically always be smaller than the

631 denominator (the total level of that taxon in the sample). However, due to amplification and other

632 technical biases, this may not practically be the case in IgA-Seq data, thus Equation 4.2 can be used to

633 account for this and ensure probability estimates fall below 1.

634

635

636
$$Prob_{ij}^{IgA^+} = \frac{IgA_{ij}^+ FracSize_j^{IgA+}}{max\left\{Whole_{ij}, IgA_{ij}^+ FracSize_j^{IgA+}\right\}}$$
(4.2)

637

638

639 This will assign a probability of 1 when the estimate of IgA+ bacteria in a taxon is larger than the

640 observed total abundance in the pre-sort sample, a reasonable assumption being that very high levels

641 of IgA binding would be necessary to produce these results.

642

643 This score only requires two additional pieces of data than the Kau and Palm indices: the taxonomic

644 abundances in the pre-sort fraction and the percentage of sorted bacteria that are in the IgA+ gate in

645 the FACS run. The latter value is already generally recorded during sorting and most IgA-Seq studies

646 to date have profiled the microbial communities from pre-sorted samples[17, 18]. Furthermore, if the

647 only interest is to identify highly bound taxa this method can negate the need to sequence the IgA-

648 fraction.

649

650 *Probability Ratio*

23

651

652   The IgA+ Probability only provides a measure of the likelihood a taxon is sufficiently bound to IgA to

653   be in the IgA+ fraction. The converse, the IgA- Probability, can also be calculated by simply

654   substituting the IgA+ abundances and fraction sizes for the IgA- values. The IgA+ and IgA-

655   probabilities can be combined to generate an IgA Probability Ratio. As both probabilities are

656   normalised to the taxon's abundance in the whole fraction it can be removed from the equation

657   (Equation 5), negating the need to sequence the pre-sort sample if desired.

658

659

$$ProbRatio_{ij} = log2\left(\frac{\left(IgA^+_{ij}FracSize_j^{IgA+}\right) + c}{\left(IgA^-_{ij}FracSize_j^{IgA-}\right) + c}\right) \quad (5)$$

661

662

663   Pseudo counts (c) must be included in the Probability Ratio to negate division by zero where taxa are

664   not observed in the IgA- fraction. Using the Probability Ratio has the benefit of capturing both

665   extremes of IgA binding within a single score (whereas the IgA+ or IgA- Probabilities are limited to

666   either direction) as well as, similar to the Kau index, centering values on zero by taking the log. This

667   provides a clear indication of whether the majority of bacteria in a taxon are found in the IgA+ or

668   IgA- fractions.

669

670   One limit of using the ratio as in Equation 5 is that the range of possible values returned is determined

671   by the pseudo count used. The magnitude of these effects can be reduced by dividing $ProbRatio$ by a

672   scaler based on the pseudo count as in Equation 6. This will bring all values within the range -1 to 1

673   with these values representing the extreme case where all bacteria are in a single fraction and belong

674   to a single taxon. Scaled Probability Ratios are used throughout.

675

$$Scaler = log2\left(\frac{1 + c}{c}\right) \quad (6)$$

677

678

679   The Palm, Kau, IgA+ Probability, and Probability Ratio scores were all calculated as defined above

680   using the *igascores* function that we have created as part of an R package IgAScores, which is

681   available at *https://github.com/microbialman/IgAScores*.

682

683   **Simulating an IgA-Seq experiment**

684

685   A simulation was used to generate IgA-Seq data where the underlying relative taxonomic binding of

686   IgA binding was known. Ten species were assigned a mean IgA binding value by random sampling

687   from an exponential distribution (raising two to the power of the generated values to increase their

688   spread). These values are arbitrary numbers that simply provide a relative IgA binding measure

689   between the species and are used as the mean to generate a normal distribution of IgA binding for

690   each species (with a standard deviation of one). For initial simulations, 30 samples were then

691   generated with random pre-sort abundances for the ten species sampled from a log normal

692   distribution.

693

694   To simulate an IgA-Seq experiment, each sample was assumed to have profiled 100,000 bacteria (a

695   reasonable magnitude for 16S rRNA gene sequencing). For each sample, the 100,000 counts were

696   assigned to one of the ten species based on the sample's species abundances. Then, for each of the

697   100,000 bacteria in each sample, a value of IgA binding was generated at random from the normal

698   distribution defined by its species mean. The distribution of IgA scores across all species was used to

699   identify values that cut off the upper and lower tails of IgA binding and these were used to define the

700   bacteria within the IgA+ and IgA- fractions respectively. The bacteria within the IgA+ and IgA-

701   fractions for each sample were then used to generate the IgA+ and IgA- relative abundances and all

702   other measures required for generating the various IgA-Seq scores.

703

704   A secondary simulation was performed to model the case where two groups are compared with a

705   consistent difference in starting abundances between them. For this, the simulation was run using the

706   same ten species as before but now considering 60 samples. Additionally, prior to generating bacterial

707   IgA binding values, 0.5 was added to the abundance of species ten in half of the samples before

708   renormalizing the abundances to sum to one. Samples with additional species ten were considered

709   cases and the unaltered samples considered controls.

710

711   All stages of the IgA-Seq simulation were carried out using the function *simulateigaseq,* which is also

712   part of the IgAScores package. All IgA-Seq indices were calculated as defined previously using the

713   *igascores* function. For simulated data experiments, a value of 10^{-6} was used for pseudo counts when

714   required as this was the same magnitude as the minimum non-zero abundance value observed in the

715   simulated data. Correlations were assessed using the *cor* function in R [36]. Between group

716   comparisons were performed using the *wilcox.test* function, adjusting p-values using *p.adjust.* Code

717   for all simulation analyses can be found at https://github.com/microbialman/IgAScoresAnalyses.

718

719

720   **Bacterial culture**

721

722   *Bacteroides thetaiotaomicron* VPI-5482 (*B. theta*) was cultured at 37°C in in brain heart infusion

723   broth supplemented with 5 μg/ml hemin and 0.5 μg/ml vitamin K (BHIS) under anaerobic conditions

724   (10% H2, 10% CO2, 80% N2). *Escherichia coli* LF82 was cultured aerobically at 37°C in Luria-

725   Bertani (LB) medium. *Helicobacter hepaticus* ATCC 51449 was grown in tryptone soya broth (TSB)

726   supplemented with 10% fetal calf serum and Skirrow Campylobacter supplements (Oxoid) under

727   microaerophilic conditions (1-3% oxygen). To stain bacteria, pure overnight cultures were pelleted by

728   centrifugation (8000 x *g*, 5 min, 4°C), washed in sterile phosphate buffered saline (PBS), and blocked

729   with filter-sterilized 10% mouse serum (10 min, ice). The following monoclonal antibodies were used

730   to stain bacteria in a 100 μl volume: mouse IgG2b anti-*E.coli* (1:100; Abcam clone 2D7/1) and mouse

731   IgA anti-*B.theta* (1:100; clone 255.4[23]). To generate the 2-member community, the optical density

732 (OD, 600 nm) and corresponding colony forming units (CFU) were determined for OD_{600} of 1: *E. coli*

733 8 x 10^7 CFU; *B. theta* 1.2 x 10^8 CFU. *Acutalibacter muris* KB18, *Akkermansia muciniphila* YL44,

734 *Bacteroides caecimuris* I48, *Bifidobacterium animalis* subsp. *animalis* YL2, *Blautia coccoides* YL58,

735 *Clostridium clostridioforme* YL32, *Clostridium innocuum* I46, *Enterococcus faecalis* KB1,

736 *Flavonifractor plautii* YL31, *Lactobacillus* I49, *Muribaculum intestinale* YL27, and *Turicimonas*

737 *muris* YL45 were used to generate stably colonized MM12 mice[37].

738

739 **Mouse strains**

740

741 All experiments were conducted in accordance with the UK Scientific Procedures Act (1986) under a

742 Project License (PPL) authorized by the UK Home Office. Animals were housed in accredited animal

743 facilities at the University of Oxford and provided with sterile water, food ad libitum, and

744 environmental enrichment. Both males and females were used in experiments after 8 weeks of age.

745 Specific pathogen-free (SPF) C57BL/6J and C57BL/6J Rag1$^{-/-}$mice were routinely tested and negative

746 for *Helicobacter* spp. and other known intestinal pathogens. Germ-free (GF) C57BL/6J mice were

747 maintained in sterile flexible film isolators and routinely screened for bacterial contamination by

748 culturing, Gram stain, and 16S PCR. GF C57BL/6J mice were stably colonized with a defined

749 consortium of 12 bacterial members, see below, of murine intestinal flora to generate a

750 sDMDMm2[26, 37] (MM12) colony that was maintained in sterile flexible film isolators. All GF and

751 MM12 mice were maintained on sterile food and water.

752

753

754 ***Helicobacter hepaticus* infection**

755

756 To induce colitis using *Helicobacter hepaticus* (*Hh*), NCI-Frederick isolate 1A strain 51449 was

757 grown as previously described [38]. Littermate control mice with MM12 flora were randomly

758 assigned to groups. Mice were fed 1.0x10^8 CFU by oral gavage on day 0 and 1. On day 0 and 7, 1mg

759 IL-10 receptor blocking antibody (clone 1B1.2) was delivered by intraperitoneal injection. Control

760   mice were housed in a separate flexible film sterile isolator and were given IL-10 receptor blocking

761   antibody in the absence of *Hh* infection.

762

763   Animals were routinely monitored for weight loss and onset of diarrhea. Mice were sacrificed at day

764   14 and processed aseptically in a class II microbiological safety cabinet. Colon contents were

765   collected for IgA-Seq and lipocalin-2 measurements (EMLCN2, Life Technologies) and stored at -

766   80°C. Formalin-fixed paraffin-embedded cross-sections of proximal, middle, and distal colon were

767   stained with hematoxylin and eosin to assess histopathology. Sections were examined for hallmarks of

768   inflammation: epithelial hyperplasia, goblet cell depletion, leukocyte infiltration, crypt abscess

769   formation, submucosal leukocyte infiltration, and interstitial edema.

770

771   **Lipocalin-2 enzyme-linked immunosorbent assay**

772

773   To prepare intestinal supernatants, 50-100 mg of colon contents were added to screw-capped O-ring

774   tubes filled with 1 ml of cOmplete ULTRA EDTA-free protease inhibitor (Roche). Samples were

775   homogenized on the TissueLyser II (Qiagen) for 10 minutes at 30 Hz and debris separated by

776   centrifugation (10,000 x g for 5 min at 4°C). Supernatant was carefully collected and either used

777   immediately or stored at -20°C. Lipocalin-2 was quantified using a mouse LCN2 enzyme-linked

778   immunosorbent assay (ELISA) kit (ThermoScientific) according to manufacturer's instructions. Each

779   sample was run in duplicate and measurements reported as ng of lipocalin per gram of sample

780

781

782   **Preparation of samples for bacterial flow cytometry**

783

784   Only sterile reagents were used to process samples. Frozen stool and intestinal contents (10-50 mg of

785   sample) were rehydrated in 1 ml of PBS and suspended by vortexing. Large debris were separated by

786   centrifugation (50 x g, 15 min, 4°C) and the clarified supernatant was passed through a 70 μm filter.

787   A 500 μl aliquot of the suspension was transferred into a new 1.5ml microcentrifuge tube and an

788   additional 1 ml of PBS added. Bacteria were pelleted (8000 x *g*, 5 min, 4°C) and blocked with 100 μl

789   of 10% rat serum (10 min, ice). An additional 1 ml of PBS was added to the blocking suspension and

790   centrifuged, and pelleted bacteria were washed with 1 ml of FACS buffer (PBS + 1% bovine serum

791   albumin). Following centrifugation, the resulting pellet was stained with PE-conjugated rat anti-

792   mouse IgA (1:100, eBioscience clone mA-6E1) in a 100 μl volume (30 min, covered on ice). Clone

793   mA-6E1 was titrated testing concentrations of 1:10, 1:20, 1:50, 1:100, 1:200, 1:500, and 1:1000.

794   Samples were washed twice with FACS buffer and resuspended in 1 ml buffer containing SYBR

795   Green I nucleic acid gel stain (1:400,000, Life Technologies) in the dark at room temperature. The

796   optimal concentration of SYBR was determined by titration testing a range from 1:100,000 to

797   1:500,000. Samples were then placed in a covered ice box and immediately acquired on the flow

798   cytometer (LSRFortessa X20 and FACSAria III, BD Biosciences).

799

800   To validate the IgA-Seq protocol, 1 ml of an overnight *B. theta* culture was first stained with mouse

801   IgA clone 255.4 (25 min, ice), washed with 1 ml PBS, followed by staining with PE-conjugated rat

802   anti-mouse IgA (1:100, eBioscience clone mA-6E1). Stained bacteria were washed three times in

803   FACS buffer before resuspension in 1 ml FACS buffer. A 500 μl aliquot of IgA-coated *B. theta* was

804   spiked into a faecal suspension prepared from specific pathogen-free (SPF) C57BL/6J mice. SYBR

805   was added to the final mixture.

806

807   **Fluorescence Activated Cell Sorting (FACS) of bacterial populations**

808

809   Samples were sorted using a FACSAria III (BD Biosciences) instrument with external aerosol

810   management. Both sample and collection tubes were maintained at 4°C. Sterile, preservative-free PBS

811   without calcium or magnesium (Invitrogen) was used for sheath fluid and was autoclaved prior to

812   sorting. The flow cytometer was sterilized according to the manufacturer's Aseptic Sort protocol to

813   decontaminate the entire sheath and sample paths. In addition, both before and after sorting, freshly

814   made 10% bleach was run for 20 min on max flow rate followed by sterile PBS for 10 min. Sheath

815   fluid from the droplet stream was collected prior to sorting as a control. Sample Line Backflush was

816   run between samples to prevent carryover.

817

818   For finer resolution of small particles including bacteria, the neutral density filter was removed and

819   threshold set to 200 for side scatter (SSC). Drop delay values were determined with the Accudrop

820   feature and were updated with each new sort setup. To sort and culture live *B. theta,* various nozzle

821   sizes (70, 85, 100 micron) and sheath pressures (20, 30, 45, 70 psi) were tested. A 10 x 10 grid was

822   programmed into the automated cell deposition unit (ACDU) stage, and *B. theta* suspended in PBS

823   was sorted in Single Cell precision mode onto BHIS agar plates for enumeration of colony forming

824   units (CFU). Nozzle sizes and sheath pressures were also tested for sort purity of IgA+ and IgA-

825   populations of faecal bacteria.

826

827   For stool and intestinal samples, the SYBR nucleic acid stain (FITC channel) helped to differentiate

828   bacteria from autofluorescent debris (BV421 or PerCP Cy5.5 channels). Samples were diluted in

829   FACS buffer containing SYBR in order to achieve an event rate of 5000-6000 events per second. To

830   begin, 100,000 events were recorded from the initial sample (pre-sort) in order to calculate the

831   percentage of bacteria in the IgA+ and IgA- gates used in the probability-based scores. Gates were

832   then drawn to delineate bacterial populations that were bound with IgA (IgA+) or unbound (IgA-).

833   The 4-way Purity precision mode was used to capture 400,000 events for each IgA+ or IgA- fraction.

834   Fractions were collected into autoclaved 2 ml screw cap tubes (ThermoFisher Scientific) pre-coated

835   with 200 μl FACS buffer. Sort purity of each fraction was recorded from 100 events, and DNA was

836   immediately extracted from the remainder. BD FACSDiva and Flowjo software (TreeStar) were used

837   for instrument setup and data analysis.

838

839   **Magnetic Activated Cell Separation (MACS)**

840

841   As a comparison with FACS, IgA-stained samples were incubated for 30 min at 4°C with anti-PE

842   microbeads (1:50, Miltenyi) in MACS buffer (0.5% bovine serum albumin and 2 mM EDTA in PBS).

843   Microbeads were titrated by testing concentrations of 1:5, 1:20, 1:50, 1:100, 1:200, 1:500. Cells were

844   pelleted by centrifugation (10,000 x g, 5 min, 4°C) and washed twice in MACS buffer before

845   resuspension in 1 ml. LS columns (Miltenyi) were placed on a magnetic stand (Miltenyi) and pre-

846   washed with 10 ml MACS buffer before the sample was loaded. Unlabelled "MACS neg" cells were

847   collected in 3 x 3 ml washes. The LS column was then removed from the magnet and the labelled

848   "MACS pos" cells were collected in 6 ml MACS buffer using the LS column plunger. MACS

849   fractions were then analysed for purity by flow cytometry.

850

851   **DNA extraction**

852

853   Only sterile molecular-grade reagents and filter-sterilized buffers were used to extract DNA. Sorted

854   fractions were centrifuged (16,000 x g, 20 min, 4°C) and the supernatant removed such that only 300

855   μl remained in the tube. For unsorted (pre-sort) samples, 100 ul was transferred into an autoclaved 2

856   ml screw cap tube containing 200 μl FACS buffer. The following was then added to each tube: 250 μl

857   autoclaved 0.1 mm zirconia/silica beads (Biospec), 300 μl Lysis buffer (200 mM NaCl; 200 mM Tris;

858   20 mM EDTA; pH 8), 200 μl 20% SDS, and 500 μl of phenol:chloroform:isoamylalcohol (PCI

859   25:24:1, pH 7.9, Sigma). Samples were bead beaten (6,500 rpm for 4 min, 3 min on ice, repeat 2x,

860   Precellys tissue homogeniser), then centrifuged (6,000 x g, 10 min, 4°C) to separate phases. The

861   aqueous phase was transferred into 5PRIME Phase Lock Gel Light tubes (Quantabio) and an equal

862   volume of PCI added. After mixing by inversion, samples were centrifuged (16,000 x g, 10 min) and

863   the aqueous phase transferred to a new Eppendorf tube. DNA was precipitated with 1/10 volume 3M

864   NaOAc (pH 5.5) and 1 volume of isopropanol overnight at -20°C. After precipitation, DNA was

865   pelleted (16,000 x g, 30 min, 4°C) and the supernatant carefully removed. The pellet was washed in

866   500 μl 70% ethanol, centrifuged (16,000 x g, 10 min, 4°C), and the wash repeated again. Residual

867   ethanol was removed from pelleted DNA and the tube placed on a 37°C heat block until the pellet was

868   completely dry. Cleaned DNA pellets were resuspended in 30 μl TE buffer at 50°C for 30 min, then

869   stored at -20°C until 16S rRNA gene library preparation.

870

871

872 **16S rRNA gene sequencing**

873

874 The V4 region of 16S ribosomal RNA gene was amplified using barcoded primer pairs[39, 40].

875 Amplicons were generated in 50 μl PCR reactions: template DNA (2 μl), 10 μM 515F primer (1 μl),

876 10 μM 806R (1 μl), 5PRIME HotMasterMix (20 μl), and water (26 μl). Water was added instead of

877 DNA for no-template controls. Thermocycler conditions: 94°C for 3 min; 35 cycles of 94°C for 45 s,

878 50°C for 60 s, and 72°C for 90 s; 72°C for 10 min. Amplicons were cleaned (UltraClean PCR Clean-

879 Up Kit, Qiagen) and quantified (Quant-iT dsDNA high-sensitivity kit, ThermoFisher) in triplicate

880 before pooling. The pooled library was precipitated with 2 volumes of 100% ethanol and a final

881 concentration of 0.2M NaCl (45 min, ice). The supernatant was removed following centrifugation

882 (7800 x g, 40 min, 4°C) and the pellet washed with 1 volume of 70% ethanol. The cleaned library was

883 pelleted (7800 x g, 20 min, 4°C) and air dried to remove residual ethanol before resuspending in 100

884 μl DNAase-free water. Gel clean-up was performed (QIAquick Gel Extraction Kit, Qiagen) and the

885 final library was sequenced on the MiSeq (Illumina) platform to generate 2 x 250 base pair paired-end

886 reads.

887

888 All 16S rRNA gene sequencing data was quality checked using FastQC and processed using DADA2

889 within the NGSKit pipeline (https://github.com/nickilott/NGSKit) to generate an amplicon sequence

890 variant (ASV) table[41]. DADA2 was used to assigned taxonomy to ASVs using a database built

891 from a combination of both the RefSeq and RDP databases[42]. ASV counts were then summarised at

892 the species level and all analyses carried out on these relative abundances (summing to one within a

893 sample).

894

895 **IgA-Seq in a mouse model of colitis**

896

897 ASV counts were generated from 16S rRNA gene sequences as described above, producing

898 54091±7970 (mean±SD) ASV counts per sample (excluding the blank control which had 5119

32

899   counts). These were summarised at the species level. Given the samples contained a known MM12

900   microbiota, the presence of unexpected species in samples and species observed in a sequencing

901   control blank were used to find an abundance threshold that removed the majority of contaminants.

902   Non-metric multi-dimensional scaling was used to visualise the relationship between samples from

903   each mouse in each fraction using the *metaMDS* function from the vegan R package[43].

904   Comparisons of IgA-Seq data were performed between the four anti-IL10R only controls and the four

905   *Hh* treated mice for the Palm, Kau and the Probability Ratio scores. These were generated using the

906   *igascores* function as for the simulated data. A pseudo count of 10^{-3} was added where necessary as

907   this was the magnitude of the lowest non-zero abundance value observed in the data.

908

909   Scores were compared between the colitic and control groups for taxa where there were at least three

910   samples scored in both groups (taxa were scored NA if they had zero abundance in both the positive

911   and negative fractions). Given the small sample size of each comparison significant differences were

912   determined by carrying out all possible permutations of group labels and observing the difference in

913   group means for each taxon for each score. The true difference in means was compared to the

914   differences across permutations to derive an exact p-value, considering significance where p<0.1.

915   This more permissive threshold was used given the small sample size (min three per group). To

916   generate comparable effect sizes between scores, which are on different scales, the difference in

917   means between groups was normalised to the standard deviations within the groups using the strictly

918   standardised mean difference, calculated using the *ssmd* function from the *phenoDist* R package [44].

919   The species level data for these analyses are made available within the *IgAScores* package and all

920   code for the analyses are available at https://github.com/microbialman/IgAScoresAnalyses.

921

922   **Analysis of Huus et al data**

923

924   Sample metadata, IgA+ and IgA- fraction sizes, and the pre-processed taxon count table used in the

925   original study were provided by the authors. The counts table was filtered to remove low abundance

926   taxa using code published with the original study and then subset to just the samples for which the

33

927   fraction sizes were available. The Kau Index and Probability Ratio scores were then generated using

928   the *igascores* function as previously. For each taxon, a two-way ANOVA was performed, using the

929   *aov* function in R, to determine if there was a difference in IgA binding score between diet treatments

930   or the interaction of diet and mouse age. This was carried out for both the Kau Index and Probability

931   Ratio, considering a taxon significant if either diet or the diet-age interaction had a nominal $p<0.05$.

932   Taxa were only tested that had scores (i.e. were not absent in both the IgA+ and IgA- fractions) in at

933   least six samples spread across all age points and both conditions. The magnitude of effects was

934   estimated as the difference in mean scores between MAL and CON for each taxon and was calculated

935   at each of the three ages individually. Mean differences were normalised by the standard deviation

936   within groups, using the strictly standardised mean difference as for the colitis analysis (to make the

937   values comparable between the Kau index and Probability Ratio). Coefficient of variation was

938   calculated within each taxon within each experimental group (age and diet combined) for each scoring

939   method and compared using a Mann-Whitney test. All code for the replication analysis can be found

940   at https://github.com/microbialman/IgAScoresAnalyses.

941
942   **Figure titles and legends**

943
944   **Figure 1. Benchmarking a protocol to isolate IgA+ and IgA- faecal bacteria by fluorescence activated cell sorting.** A)
945   IgA-Seq gating strategy. Faecal bacteria from SPF C57BL/6 mice stained with anti-mouse IgA (PE). Gating on a population
946   based on FSC and SSC characteristics, followed by discrimination of SYBR+ (FITC) bacteria from autofluorescent (PerCP
947   Cy5.5) debris. IgA+ and IgA- populations were sorted from SYBR+ cells. B) Viability of B. theta (*Bt*) collected by various
948   nozzle sizes (μm) and sheath pressures (psi) on the FACSAria III. Culture-grown *Bt* was stained with mouse anti-*Bt* IgA
949   (clone 255.4) and rat anti-mouse IgA (PE, clone mA-6E1). 100 cells were plated in Single Cell precision mode onto BHIS
950   agar plates for enumeration of colony forming units (CFU). C) IgA+ and IgA- fractions were collected from SPF C57BL/6J
951   mice (n=3). *Left:* percentage of IgA+ faecal bacteria detected in each collected fraction for a range of nozzle and pressure
952   configurations. *Right:* sort purities for these configurations defined by the percentage of events that remained in the
953   designated sort gates. Lines represent means with SEM. D) A portion of the IgA-stained faecal suspensions from Fig. 2A
954   were also separated into IgA+ and IgA- fractions by magnetic activated cell separation (MACS) as a comparison. PE IgA-
955   stained samples were incubated with anti-PE microbeads and fractions collected by LS column separation. Representative
956   flow cytometry plots of the starting material in SPF stool and the IgA+ and IgA- fraction isolated by FACS and MACS. E)
957   MACS purity of collected fractions as determined by flow cytometry, technical triplicates from the same stool suspension.

958
959   **Figure 2. Testing IgA-Seq specificity in a complex faecal microbial community.** Culture-grown *Bt* was stained with
960   mouse anti-*Bt* IgA (clone 255.4) and rat anti-mouse IgA (PE, clone mA-6E1), then spiked into an unstained faecal
961   suspension prepared from SPF C57BL/6J mice with a complex microbiota. A) Experimental design and sort setup, gated on
962   SYBR+ cells. B) Sorts repeated on the same *Bt*-stool suspension to generate technical triplicates. *Left:* percentage of IgA+
963   bacteria in the pre-sorted sample, IgA+ and IgA- fractions. *Right:* purity check on the collected fractions. Lines represent
964   means with SEM. C) Taxa abundances based on 16S rRNA gene sequencing of a complex stool microbiome (triplicate
965   sequencing replications stool 1-3), triplicate sorted IgA+ fractions (sort 1-3), and *Bt* genomic DNA (*Bt* gDNA). Top 10
966   genera are shown. D) Relative abundance of *Bt* ASV399 in sorted samples.

967
968   **Figure 3. The influence of pre-sort abundances on existing IgA-Seq scores can be overcome using probability-based**
969   **approaches.** A) A toy example where two samples have two species with the same IgA binding profiles but different
970   starting abundances. B) The distribution of arbitrary IgA binding values used for the ten species in the IgA-Seq simulations,
971   dashed lines indicate the IgA+ and IgA- fraction thresholds. Species coloured as in C. C) The species abundances in the pre-
972   sorted, IgA+ and IgA- samples for the 30 samples simulated. D) The size of the IgA+ and IgA- fractions in the simulated

973 samples as a percentage of their total bacteria. E) Comparison of variance in IgA binding estimates across samples using
974 each scoring approach. Coefficient of variance was calculated for each species individually. ** = p<0.01, **** = p<0.0001
975 in Mann-Whitney tests after FDR correction. Boxes represent the median and interquartile range (IQR) and the whiskers the
976 largest and smallest values within one and half IQR of the upper and lower IQR limits. F) Pearson and Spearman
977 correlations between the true mean IgA binding scores used to simulate data and the scores estimated by each of the different
978 indices.
979
980 **Figure 4. The probability ratio overcomes pre-sort abundance biases when carrying out between-group comparisons.**
981 A) Simulations were carried out as in Figure 4 (Controls) with an additional 30 samples that were initiated with the
982 additional abundance of Species 10 (Cases). Abundances in the pre-sort, IgA+, and IgA- fractions using the thresholds as in
983 Figure 4A. B) Differences in the IgA+ and IgA- fraction sizes as a percentage of total bacteria between cases and controls.
984 P-value shown from Mann-Whitney tests. C) Heatmaps showing the scores estimated by the Kau and Probability Ratios
985 across all samples. D) Comparison of IgA binding scores for the ten species in cases and controls when using either the Kau
986 score or the Probability Ratio. Significant differences are highlighted with * (FDR adjusted Mann-Whitney p<0.05) and
987 species are ordered by true IgA binding value. In all boxplots the boxes represent the median and interquartile range and the
988 whiskers the largest and smallest values within one and half IQR of the upper and lower IQR limits. In D, points outside this
989 range are shown.
990
991 **Figure 5. IgA-Seq in a mouse model of colitis with a defined 12-member microbiota.** MM12 mice were administered
992 weekly injections of anti-IL10R (day 0, 7). Controls received anti-1L10R alone (aIL10R, n=4), and the colitis group were
993 additionally infected with *H. hepaticus* at the start of the experiment (Hh+aIL10R, n=4). A) Experimental design and
994 representative colon histology with haematoxylin and eosin staining. B) Mouse lipocalin-2 ELISA as a measure of colonic
995 inflammation. Lines at means and SEM. **p<0.01 unpaired Mann-Whitney test, ns= non-significant. SS represents steady
996 state mice with no aIL10R exposure. C) Representative flow cytometry plots of the percentage of colonic MM12 bacteria
997 coated by IgA. D) Percentage of bacteria coated by host IgA and subjected to IgA-Seq. P-values represent Mann-Whitney
998 tests. E) Relative abundance plots showing the MM12 species in each sample. Each row represents an individual animal. F)
999 Non-metric multi-dimensional scaling of pre-sort, IgA+, and IgA- fractions from Bray-Curtis distances. G) *Left:* means and
1000 95% confidence intervals of IgA binding scores significantly different between groups. Significance determined by complete
1001 permutation of group labels where, exact permuted p<0.1). *Right:* Mean difference of scores between groups (colitic -
1002 control). Mean is normalised by its standard deviation for comparability between scoring methods (using the strictly
1003 standardised mean difference SSMD). H) *Left*: boxplots of *A. muciniphila* relative abundance. *Centre*: boxplots of IgA+
1004 fraction size. *Right:* boxplots of adjustment for the difference in fraction size (abundance in the IgA+ fraction size multiplied
1005 by *A. muciniphila* abundance). In the boxplots in D and H, boxes represent the median and IQR and the whiskers the largest
1006 and smallest values within one and half IQR of the upper and lower IQR limits.

1007 **Figure 6. Increased power when using the Probability Ratio to reanalyse data from Huus et al. 2020.** A) Boxplots
1008 showing the Kau index scores at each age for all taxa that were significantly different by either diet or the interaction of age
1009 and diet in two-way ANOVAs (nominal p<0.05). Each plot shows which of diet and the diet:age interaction were significant
1010 and their p-values. Boxes represent the median and IQR and the whiskers the largest and smallest values within one and half
1011 IQR of the upper and lower IQR limits. UC represents taxa that were unclassified below the given taxonomy. B) Plot as in A
1012 but for the Probability Ratio scores. C) Left: Scatterplot of the p-values for all the comparisons that were significant in either
1013 A or B showing the p-value when using the Probability Ratio (y) or Kau Index (x). The red-line shows y=x, highlighting the
1014 lower p-values in the Probability Ratio tests. Right: Scatterplot as for p-values but showing the effect size (difference in
1015 means between the two diets) at each of the three ages for all of the significant comparisons in A and B. Effect size is
1016 quantified as the strictly standardised mean difference (MAL-CON). D) Boxplots comparing the absolute coefficient of
1017 variation of each taxon's score within each experimental group (for all taxa detected in the Huus et al. dataset) when using
1018 either the Kau Index or Probability Ratio. Significance shown from Mann-Whitney U test.
1019
1020 **Declarations**
1021
1022 **Ethics approval and consent to participate**

1023 All animal experiments were conducted in accordance with the UK Scientific Procedures Act (1986) under a

1024 Project License (PPL) authorized by the UK Home Office.

1025 **Consent for publication**

1026 Not applicable

1027

1028 **Availability of data and materials**

35

1029 All code for the analyses in this study are available at https://github.com/microbialman/IgAScoresAnalyses. The

1030 IgAScores package is available at *https://github.com/microbialman/IgAScores* and also includes a pre-processed

1031 version of the data used in the analyses of the colitis model. The raw 16S rRNA gene sequencing data for the

1032 colitis experiment are available at the European Nucleotide Archive under study accession PRJEB39814

1033 (https://www.ebi.ac.uk/ena/browser/view/PRJEB39814).

Competing interests

1035 The authors declare that they have no competing interests.

Funding

Authors' contributions

1046 MAJ, CP, FP, LHL contributed to study design. MAJ,NEI,LHL contributed to data analyses.

1047 CP,ANH,JW,AJM,LHL contributed to experimental work. MAJ,KEH,BF contributed to replication analyses.

1048 MAJ,LHL authored the manuscript with inputs from all authors.

Acknowledgements

1055
1056
1057
1058
1059
1060
1061
1062

References

1. Sommer F, Bäckhed F. The gut microbiota — masters of host development and physiology. Nat Rev Microbiol. 2013;11:227–38. doi:10.1038/nrmicro2974.

2. Macpherson AJ, McCoy KD, Johansen F-E, Brandtzaeg P. The immune geography of IgA induction and function. Mucosal Immunol. 2008;1:11–22. doi:10.1038/mi.2007.6.

3. Gutzeit C, Magri G, Cerutti A. Intestinal IgA production and its role in host-microbe interaction. Immunol Rev. 2014;260:76–85. doi:10.1111/imr.12189.

4. Phalipon A, Cardona A, Kraehenbuhl JP, Edelman L, Sansonetti PJ, Corthésy B. Secretory component: a new role in secretory IgA-mediated immune exclusion in vivo. Immunity. 2002;17:107–15. doi:10.1016/s1074-7613(02)00341-2.

5. Macpherson AJ, Köller Y, McCoy KD. The bilateral responsiveness between intestinal microbes and IgA. Trends Immunol. 2015;36:460–70. doi:10.1016/j.it.2015.06.006.

6. Donaldson GP, Ladinsky MS, Yu KB, Sanders JG, Yoo BB, Chou W-C, et al. Gut microbiota utilize immunoglobulin A for mucosal colonization. Science (80-). 2018;360:795–800. doi:10.1126/science.aaq0926.

7. Ansaldo E, Slayden LC, Ching KL, Koch MA, Wolf NK, Plichta DR, et al. Akkermansia muciniphila induces intestinal adaptive immune responses during homeostasis. Science (80-). 2019;364:1179–84. doi:10.1126/science.aaw7479.

8. Moor K, Diard M, Sellin ME, Felmy B, Wotzka SY, Toska A, et al. High-avidity IgA protects the intestine by enchaining growing bacteria. Nature. 2017;544:498–502. doi:10.1038/nature22058.

9. Mantis NJ, Rol N, Corthésy B. Secretory IgA's complex roles in immunity and mucosal homeostasis in the gut. Mucosal Immunol. 2011;4:603–11. doi:10.1038/mi.2011.41.

10. Grasset EK, Chorny A, Casas-Recasens S, Gutzeit C, Bongers G, Thomsen I, et al. Gut T cell–independent IgA responses to commensal bacteria require engagement of the TACI receptor on B cells. Sci Immunol. 2020;5:eaat7117. doi:10.1126/sciimmunol.aat7117.

11. Macpherson AJ, Gatto D, Sainsbury E, Harriman GR, Hengartner H, Zinkernagel RM. A primitive T cell-independent mechanism of intestinal mucosal IgA responses to commensal bacteria. Science. 2000;288:2222–6. doi:10.1126/science.288.5474.2222.

12. Bunker JJ, Flynn TM, Koval JC, Shaw DG, Meisel M, McDonald BD, et al. Innate and Adaptive Humoral Responses Coat Distinct Commensal Bacteria with Immunoglobulin A. Immunity. 2015;43:541–53. doi:10.1016/j.immuni.2015.08.007.

13. Bunker JJ, Erickson SA, Flynn TM, Henry C, Koval JC, Meisel M, et al. Natural polyreactive IgA antibodies coat the intestinal microbiota. Science (80-). 2017;358.

14. Wei M, Shinkura R, Doi Y, Maruya M, Fagarasan S, Honjo T. Mice carrying a knock-in mutation of Aicda resulting in a defect in somatic hypermutation have impaired gut homeostasis and compromised mucosal defense. Nat Immunol. 2011;12:264–70. doi:10.1038/ni.1991.

15. Tsuruta T, Inoue R, Iwanaga T, Hara H, Yajima T. Development of a method for the identification of S-IgA-coated bacterial composition in mouse and human feces. Biosci Biotechnol Biochem. 2010;74:968–73. doi:10.1271/bbb.90801.

16. Kullberg MC, Ward JM, Gorelick PL, Caspar P, Hieny S, Cheever A, et al. Helicobacter hepaticus Triggers Colitis in Specific-Pathogen-Free Interleukin-10 (IL-10)-Deficient Mice through an IL-12- and Gamma Interferon-Dependent Mechanism. Infect Immun. 1998;66:5157–66. doi:10.1128/IAI.66.11.5157-5166.1998.

17. Palm NW, de Zoete MR, Cullen TW, Barry NA, Stefanowski J, Hao L, et al. Immunoglobulin A Coating Identifies Colitogenic Bacteria in Inflammatory Bowel Disease. Cell. 2014;158:1000–10. doi:10.1016/j.cell.2014.08.006.

18. Kau AL, Planer JD, Liu J, Rao S, Yatsunenko T, Trehan I, et al. Functional characterization of IgA-targeted bacterial taxa from undernourished Malawian children that produce diet-dependent enteropathy. Sci Transl Med. 2015;7:276ra24-276ra24. doi:10.1126/scitranslmed.aaa4877.

19. Viladomiu M, Kivolowitz C, Abdulhamid A, Dogan B, Victorio D, Castellanos JG, et al. IgA-coated E. Coli enriched in Crohn's disease spondyloarthritis promote TH17-dependent inflammation. Sci Transl Med. 2017;9.

20. Huus KE, Bauer KC, Brown EM, Bozorgmehr T, Woodward SE, Serapio-Palacios A, et al. Commensal Bacteria Modulate Immunoglobulin A Binding in Response to Host Nutrition. Cell Host Microbe. 2020;:1–13. doi:10.1016/j.chom.2020.03.012.

21. Kawamoto S, Maruya M, Kato LM, Suda W, Atarashi K, Doi Y, et al. Foxp3+ T Cells Regulate Immunoglobulin A Selection and Facilitate Diversification of Bacterial Species Responsible for Immune Homeostasis. Immunity. 2014;41:152–65. doi:10.1016/j.immuni.2014.05.016.

22. Catanzaro JR, Strauss JD, Bielecka A, Porto AF, Lobo FM, Urban A, et al. IgA-deficient humans exhibit gut microbiota dysbiosis despite secretion of compensatory IgM. Sci Rep. 2019;9:13574. doi:10.1038/s41598-019-49923-2.

23. Peterson DA, McNulty NP, Guruge JL, Gordon JI. IgA Response to Symbiotic Bacteria as a Mediator of

1123   Gut Homeostasis. Cell Host Microbe. 2007;2:328–39. doi:10.1016/j.chom.2007.09.013.

1124   24. Kullberg MC, Jankovic D, Gorelick PL, Caspar P, Letterio JJ, Cheever AW, et al. Bacteria-triggered CD4+
1125   T Regulatory Cells Suppress Helicobacter hepaticus–induced Colitis. J Exp Med. 2002;196:505–15.
1126   doi:10.1084/jem.20020556.

1127   25. Krausgruber T, Schiering C, Adelmann K, Harrison OJ, Chomka A, Pearson C, et al. T-bet is a key
1128   modulator of IL-23-driven pathogenic CD4+ T cell responses in the intestine. Nat Commun. 2016;7:11627.
1129   doi:10.1038/ncomms11627.

1130   26. Brugiroux S, Beutler M, Pfann C, Garzetti D, Ruscheweyh H-J, Ring D, et al. Genome-guided design of a
1131   defined mouse microbiota that confers colonization resistance against Salmonella enterica serovar
1132   Typhimurium. Nat Microbiol. 2017;2:16215. doi:10.1038/nmicrobiol.2016.215.

1133   27. Stallhofer J, Friedrich M, Konrad-Zerna A, Wetzke M, Lohse P, Glas J, et al. Lipocalin-2 Is a Disease
1134   Activity Marker in Inflammatory Bowel Disease Regulated by IL-17A, IL-22, and TNF-α and Modulated by
1135   IL23R Genotype Status. Inflamm Bowel Dis. 2015;21:1. doi:10.1097/MIB.0000000000000515.

1136   28. Palm NW, de Zoete MR, Cullen TW, Barry NA, Stefanowski J, Hao L, et al. Immunoglobulin A Coating
1137   Identifies Colitogenic Bacteria in Inflammatory Bowel Disease. Cell. 2014;158:1000–10.
1138   doi:10.1016/j.cell.2014.08.006.

1139   29. Lin R, Chen H, Shu W, Sun M, Fang L, Shi Y, et al. Clinical significance of soluble immunoglobulins A
1140   and G and their coated bacteria in feces of patients with inflammatory bowel disease. J Transl Med.
1141   2018;16:359. doi:10.1186/s12967-018-1723-0.

1142   30. Castro-Dopico T, Dennison TW, Ferdinand JR, Mathews RJ, Fleming A, Clift D, et al. Anti-commensal IgG
1143   Drives Intestinal Inflammation and Type 17 Immunity in Ulcerative Colitis. Immunity. 2019;50:1099-1114.e10.
1144   doi:10.1016/j.immuni.2019.02.006.

1145   31. Simón-Soro Á, D'Auria G, Collado MC, Džunková M, Culshaw S, Mira A. Revealing microbial recognition
1146   by specific antibodies. BMC Microbiol. 2015;15:132. doi:10.1186/s12866-015-0456-y.

1147   32. Wilmore JR, Gaudette BT, Gomez Atria D, Hashemi T, Jones DD, Gardner CA, et al. Commensal Microbes
1148   Induce Serum IgA Responses that Protect against Polymicrobial Sepsis. Cell Host Microbe. 2018;23:302-
1149   311.e3. doi:10.1016/j.chom.2018.01.005.

1150   33. Acinas SG, Sarma-Rupavtarm R, Klepac-Ceraj V, Polz MF. PCR-Induced Sequence Artifacts and Bias:
1151   Insights from Comparison of Two 16S rRNA Clone Libraries Constructed from the Same Sample. Appl
1152   Environ Microbiol. 2005;71:8966–9. doi:10.1128/AEM.71.12.8966-8969.2005.

1153   34. Louca S, Doebeli M, Parfrey LW. Correcting for 16S rRNA gene copy numbers in microbiome surveys
1154   remains an unsolved problem. Microbiome. 2018;6:41. doi:10.1186/s40168-018-0420-9.

1155   35. Johnson JS, Spakowicz DJ, Hong B-Y, Petersen LM, Demkowicz P, Chen L, et al. Evaluation of 16S rRNA
1156   gene sequencing for species and strain-level microbiome analysis. Nat Commun. 2019;10:5029.
1157   doi:10.1038/s41467-019-13036-1.

1158   36. R Development Core Team. R: A language and environment for statistical computing. Vienna, Austria: R
1159   Foundation for Statistical Computing; 2009.

1160   37. Li H, Limenitakis JP, Fuhrer T, Geuking MB, Lawson MA, Wyss M, et al. The outer mucus layer hosts a
1161   distinct intestinal microbial niche. Nat Commun. 2015;6:8292. doi:10.1038/ncomms9292.

1162   38. Maloy KJ, Salaun L, Cahill R, Dougan G, Saunders NJ, Powrie F. CD4+CD25+ TR Cells Suppress Innate
1163   Immune Pathology Through Cytokine-dependent Mechanisms. J Exp Med. 2003;197:111–9.
1164   doi:10.1084/jem.20021345.

1165   39. Caporaso JG, Lauber CL, Walters WA, Berg-Lyons D, Huntley J, Fierer N, et al. Ultra-high-throughput
1166   microbial community analysis on the Illumina HiSeq and MiSeq platforms. ISME J. 2012;6:1621–4.
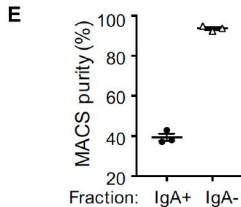1167   doi:10.1038/ismej.2012.8.

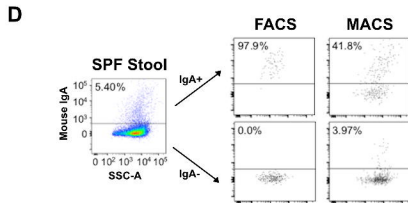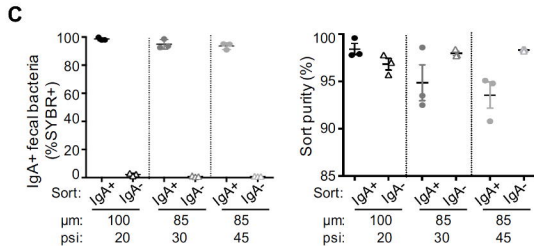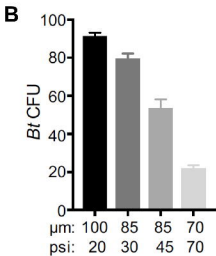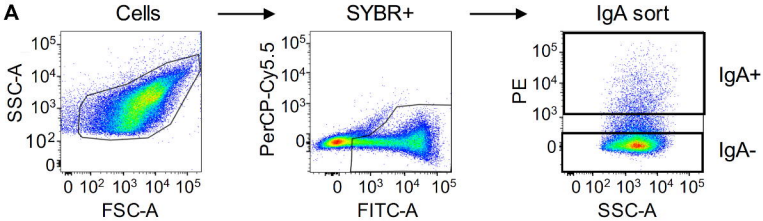1168   40. Apprill A, McNally S, Parsons R, Weber L. Minor revision to V4 region SSU rRNA 806R gene primer
1169   greatly increases detection of SAR11 bacterioplankton. Aquat Microb Ecol. 2015;75:129–37.
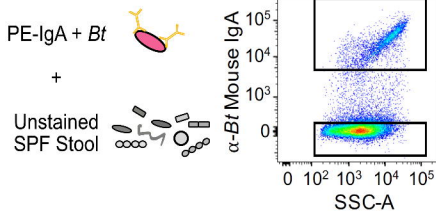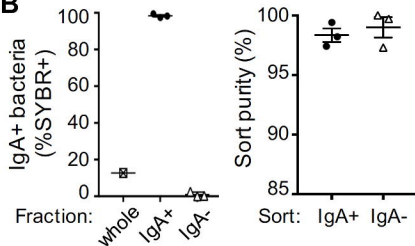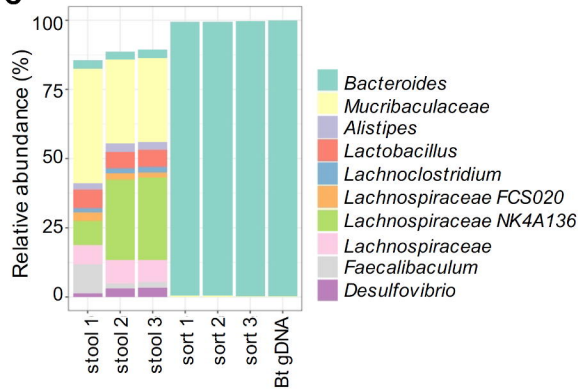1170   doi:10.3354/ame01753.

1171   41. Callahan BJ, McMurdie PJ, Rosen MJ, Han AW, Johnson AJA, Holmes SP. DADA2: High-resolution
1172   sample inference from Illumina amplicon data. Nat Methods. 2016;13:581–3. doi:10.1038/nmeth.3869.

1173   42. Alishum A. DADA2 formatted 16S rRNA gene sequences for both bacteria & archaea. 2019.
1174   doi:10.5281/ZENODO.2541239.

1175   43. Dixon P. VEGAN, a package of R functions for community ecology. J Veg Sci. 2003;14:927–30.
1176   doi:10.1111/j.1654-1103.2003.tb02228.x.

1177   44. Zhang X, Boutros M. A novel phenotypic dissimilarity method for image-based high-throughput screens.
1178   BMC Bioinformatics. 2013;14:336. doi:10.1186/1471-2105-14-336.

1179

A Cells → SYBR+ → IgA sort

B *Bt* CFU

C IgA+ fecal bacteria (%SYBR+) | Sort purity (%)

D SPF Stool | FACS | MACS

E MACS purity (%)

A

PE-IgA + *Bt*
+
Unstained
SPF Stool

α-*Bt* Mouse IgA

SSC-A

Sort

B

IgA+ bacteria (%SYBR+)

Fraction: whole IgA+ IgA−

Sort purity (%)

Sort: IgA+ IgA−

C

Relative abundance (%)

stool 1 stool 2 stool 3 sort 1 sort 2 sort 3 Bt gDNA

Bacteroides
Muribaculaceae
Alistipes
Lactobacillus
Lachnoclostridium
Lachnospiraceae FCS020
Lachnospiraceae NK4A136
Lachnospiraceae
Faecalibaculum
Desulfovibrio

D

Bt ASV399 abundance (%)

stool 1 stool 2 stool 3 sort 1 sort 2 sort 3 Bt gDNA